NASA Contractor Report 178245

Application of CARS to Scramjet Combustion

(NASA-CR-178245) APPLICATION OF CARS TO SCRAMJET COMBUSTION Final Report (Systems Research Labs., Inc.) 32 p CSCL 07D

N87-20400

Unclas
G3/25 45354

Richard R. Antcliff

Research Applications Division
Systems Research Laboratories, Inc.
2800 Indian Ripple Road
Dayton, OH 45440-3696

Contract NAS1-16562

April 1987

National Aeronautics and
Space Administration

Langley Research Center
Hampton, Virginia 23665-5225

Preface

This final report was prepared by the Research Applications Division of Systems Research Laboratories, Inc., under NASA Contract NAS1-16562, with Dr. G. Burton Northam as NASA Project Monitor. The research was conducted by Dr. Richard R. Antcliff. This report describes efforts performed during the period 12 March 1981 through 2 October 1986.

TABLE OF CONTENTS

LIST OF ILLUSTRATIONS

INTRODUCTION

Physical probes have provided combustion researchers with temperature and pressure information for many years. However, interference with the flow properties and degradation in hostile environments limit the use of probes. Optical diagnostic techniques generally overcome these limitations. One of these techniques, coherent anti-Stokes Raman scattering (CARS), has the additional advantages of (1) high conversion efficiency, (2) a laser-like beam for high collection efficiency, fluorescence, and luminosity discrimination, and (3) high spatial and temporal resolution. These advantages must be weighed against the increased complexity of a CARS system and its limitations. These limitations include the presence of an interfering nonresonant background, the need for optical access, and the requirements for stability of the optical system. CARS has been applied to many complex environments including plasmas,[1,2] internal combustion engines,[3,4] shock tubes,[5,6] full-scale combustors,[7-13] and a supersonic combustor.[14]

This report describes a system which has been developed at NASA Langley Research Center for simultaneous measurement of temperature and nitrogen and oxygen number density. The system has been described, in part, previously[15-18] as specific subsystems were developed. This system has been utilized to obtain a data base for comparison with computational-fluid-dynamics (CFD) calculations. These data have been included to illustrate the capabilities of the system.

THEORETICAL BACKGROUND

A CARS signal is generated as two laser beams at frequency ω_1 and one laser beam at frequency ω_2 are mixed to produce a fourth laser-like beam at the CARS frequency $\omega_3 = 2\omega_1 - \omega_2$. The CARS signal is dependent upon the polarizability of the molecule. The polarizability can be written as a power series[19]

$$P = \chi^{(1)}E + \chi^{(2)}E^2 + \chi^{(3)}E^3 + \text{H.O.T.} \qquad (1)$$

where E is the electric field strength and $\chi^{(1)}$ is the susceptibility. It is the third-order terms which describe CARS and other nonlinear Raman techniques. The intensity of the CARS signal, I_3, has been shown[20] to be

$$I_3 = \left(\frac{4\pi^2\omega_3}{C^2 n^3}\right)^2 I_1^2 I_2 L^2 (3\chi^{(3)})^2 \qquad (2)$$

where I_1 is the intensity at frequency ω_1; C is the speed of light; n_3 is the refractive index at ω_3; and L is the interaction length. This equation assumes that the required momentum phase matching has been satisfied and that the beams have the same focal diameter. The nonlinear susceptibility is a complex term[21] which has been simplified for normal CARS conditions[20,22]

$$\chi^{(3)} = \frac{N}{4\hbar^3} \sum_{v,J} \frac{\Delta_{v,J}(d\sigma/d\Omega)_{v,J}}{\omega_r - (\omega_1 - \omega_2) - i\Gamma_{v,J}} + \chi_B^{(3)} \qquad (3)$$

where N is the number density of the species probed; $\Delta_{v,J}$ is the population difference between the states studied; $d\sigma/d\Omega$ is the Raman cross section and assumed to be constant; ω_r is the frequency of a Raman active rotational or vibrational state; $\Gamma_{v,J}$ is the Raman halfwidth; and $\chi_B^{(3)}$ is a collection of susceptibility terms which are generally a slowly varying function of frequency. The $\chi_B^{(3)}$ term can become important under resonance[23] conditions, when near other rotational or vibrational transitions,[24] or when the species density is low.[25]

From Eq. (3) it can be seen that as the difference between ω_1 and ω_2 approaches a Raman resonance, the signal increases dramatically. Normally ω_1 is held fixed, and ω_2 is scanned to generate a CARS spectrum. However, in turbulent environments this is impractical since the sample changes rapidly. An alternative method[26] makes use of a broadband dye laser for ω_2. Utilizing an array detector allows the complete spectrum to be acquired in a single 10-ns laser shot.

CARS SYSTEM

The CARS system at NASA Langley employs a Nd:YAG laser, broadband dye lasers, nonplanar BOXCARS beam alignment, a reference signal generated in ambient air, and both photomultiplier-tube (PMT) and photodiode-array detection. Figure 1 is a schematic diagram of the optical layout and will be referenced in the following description.

Laser System

The main pump laser was a Quanta-Ray DCR-1 Nd:YAG laser. This laser is normally operated at 10 Hz and emits $\sim$ 200 mJ in a 10-ns pulse at 532 nm. The laser has been updated with new pump cavities and O-ring seals. The 532-nm output was produced with a Quanta-Ray HG-2 temperature-controlled frequency doubler. The temperature control is helpful in eliminating repeated tweaking of the crystal angle as the crystal heats up. The 532-nm output was separated from the residual 1064-nm output by means of a Pellin-Broca prism. The residual output was directed through a second frequency doubler to obtain an additional 532-nm laser beam. This portion of the 532-nm beam was used to pump the 580-nm dye-laser oscillator.

Two broadband ($\sim$ 200 cm^{-1}) dye lasers were employed in this system. The oscillator of these dye lasers consists of a flowing dye cell oriented at Brewster's angle relative to the dye-laser optical axis. The oscillator was pumped slightly off axis in a cavity formed by a total and a 30% reflector. A single amplifier stage was used for each dye laser. Several combinations of dye-laser concentrations and pump-laser energies were used in the oscillators and amplifiers to ascertain the optimum beam quality, power output, and stability. No advantage was found over using a simple 50/50 split of the laser energy between the oscillator and amplifier and the same dye concentration in both.

The nitrogen-dye-laser (606.5 nm) concentration was $\sim$ 7.5×10^{-5} molar rhodamine 640 in methanol. The oxygen-dye-laser (508 nm) concentration was $\sim$ 5×10^{-5} molar rhodamine B in ethanol. The output frequency of these lasers can be adjusted by altering the concentration of the dye.

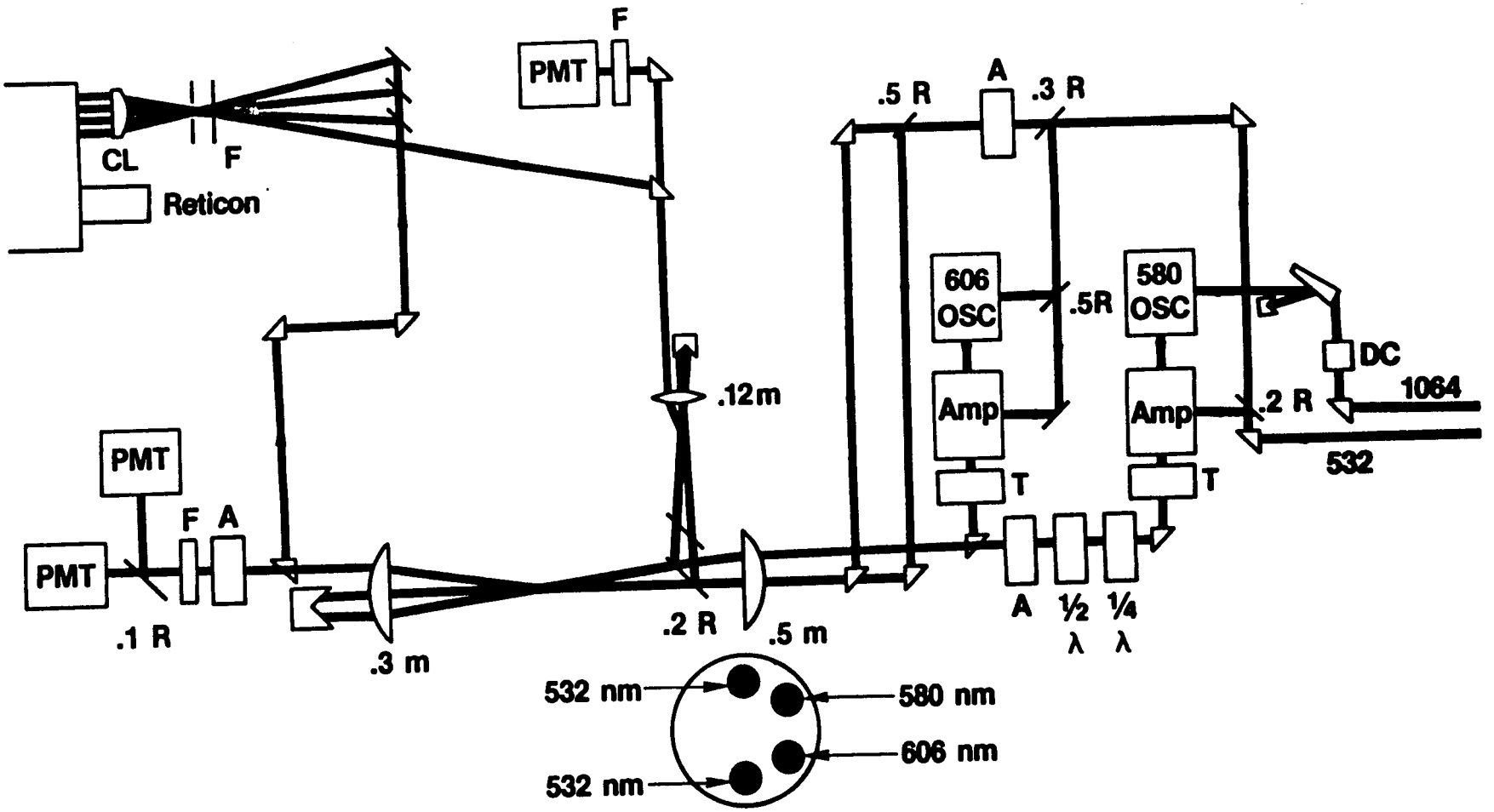

Figure 1. CARS Schematic. DC - doubling crystal, R - dichroic mirror, F - filter, A - polarization analyzer, T - telescope, 1/2λ - half-wave plate, 1/4λ - quarter-wave plate, CL - cylindrical lens.

Signal Generation

A nonplanar BOXCARS[27,28] beam configuration was used to maximize the spatial resolution of the system while maintaining optimum signal-generation efficiency. Figure 2 shows the laser-beam configuration about the focus. The 532-nm "pump" laser was split into two equal beams and positioned vertically on the focusing lens. The two dye-laser beams were positioned vertically but placed to one side of the "pump" beams. The dye-laser beams should be slightly outside an imaginary circle on the lens having a diameter equal to the "pump"-beam separation and a midpoint at the center of the lens. With this configuration the signal beams were spatially separated from the input laser beams, and the input beams could be readily trapped. The crossing and focusing element was a plano-convex 50-cm lens.

A small nitrogen jet was used to obtain the experimental interaction length. This jet, surounded by an argon sheath, was stepped through the interaction length and the signal recorded by measuring the signal to 10% on either side of the peak. The effective signal-generation length of $\sim$ 1 mm was determined. The interaction volume was assumed to be a cylinder having a diameter of 250 μm.

Referencing

Measurements obtained from a stable environment (e.g., ambient air) showed considerable fluctuation in the signal intensity. This fluctuation was due to several factors including shot-to-shot pump-laser fluctuations (both in intensity and frequency), variations in the broadband dye laser output due to mode competition, and movement of the beams causing changes in the interaction length and in the detector response. This fluctuation presented a problem in making concentration measurements since such measurements are dependent on the signal intensity. To alleviate this problem a referening system was established to compensate for variation in the signal-generation efficiency.[29] A 20% beam splitter was placed immediately after the crossing and focusing lens. This splitter, placed at 45 deg., formed a second focal volume in ambient air. The nitrogen and oxygen signals generated in this reference volume

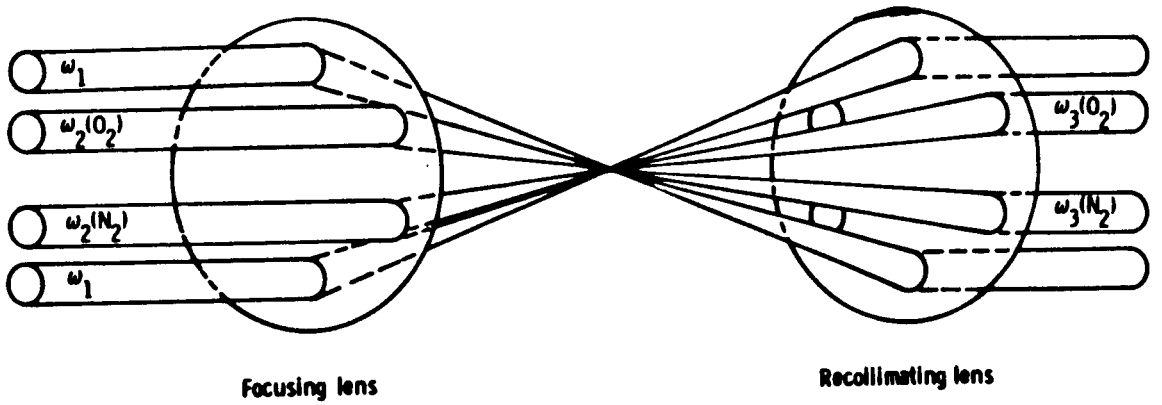

Figure 2. Focal configuration. Four laser beams enter from left and six exit at right.

and the signals generated from the data (flame) volume were detected simultaneously. A flat glass plate was placed immediately after the splitter in the reference leg to compensate for a path difference in the sample leg caused by the splitter. The reference leg was optically adjusted to produce optimum correlation between the sample and reference signals. This was accomplished through use of a real-time program which displayed the correlation as the system was adjusted. Typical correlations were better than 10% for the nitrogen signals and better than 4% for the oxygen signals.

Nitrogen Detection

The complete nitrogen Q-branch spectrum was generated with a broadband dye laser. An intensified-silicon-photodiode (ISPD) array was used in this system to capture a complete spectrum with each laser shot. The electronic scanning of this array of diodes was controlled by a minicomputer as described below. A 1-m monochromator was used in front of the detector to disperse the input beam and, thereby, reject stray laser light.

A study was made to determine the experimental dynamic range of the ISPD.[18] Using calibrated sources the actual dynamic range of the instrument was found to be $\sim$ 100. Two major factors contributed to this small measured range. First, detector noise limited the lower measurable limit to about 200 counts. Secondly, the spherical lens normally used to focus the CARS signal onto the detector was found to cause local saturation of the microchannel plate intensifier since the full detector height was not utilized. This dynamic range was insufficient for tracking the large signal-intensity variations associated with turbulent combustion.

Two modifications were made to the system to increase this dynamic range. First, the spherical lens at the entrance to the detector monochromator was replaced by a cylindrical lens. This lens produced a line image on the detector, thereby utilizing the full detector height. This improvement reduced the local saturation of the microchannel plate

intensifier and improved the linear dynamic range by approximately a factor of five. The second improvement was the implementation of an external splitter arrangement as suggested by Goss.[30] The nitrogen CARS signal was directed through a series of splitters to produce three separate signal beams having intensities of ∿ 1, 19, and 80% of the original signal. The monochromator entrance slit was rotated to the horizontal position and opened fully. The three signals were imaged side by side onto the slit plane. The signals followed the path of the monochromator and were imaged side by side on the detector. This allowed the three intensity signals to be recorded simultaneously by the diode array detector and increased the dynamic range by a factor of 100, which was sufficient for these studies. The reference nitrogen signal was also imaged onto the horizontal slit. Thus, four separate spectra were simultaneously recorded by the array detector.

Oxygen Detection

RCA 8575 Photomultipliers (PMTs) were used to detect the oxygen signals since only the integrated intensity of the signal was required. Measurements of the oxygen density are complicated by the presence of a nonresonant background signal at low oxygen densities. In this system the nonresonant background signal has been nearly eliminated by use of polarization selection.[31] The polarization characteristics of the resonant and nonresonant signals are different due to the electronic origin of the nonresonant signal. To take advantage of this difference, the polarization of the oxygen dye laser was rotated 60 deg. relative to the pump polarization. This was accomplished with a Karl Lambrecht 1/2-wave Fresnel Rhomb and a polarizing prism. A zero-order 1/4-wave retarder was also placed in the beam path to minimize elliptical polarization introduced by multiple optical elements. A polarizing prism was placed in the pump beam to improve the polarization characteristics of the beam.

With the scheme discussed above, the polarization of the resonant signal is the same as that of the pump beams (Fig. 3). The nonresonant signal, however, was rotated 30 deg. from the pump beam. The nonresonant signal was blocked by placing an analyzer orthogonal to the nonresonant

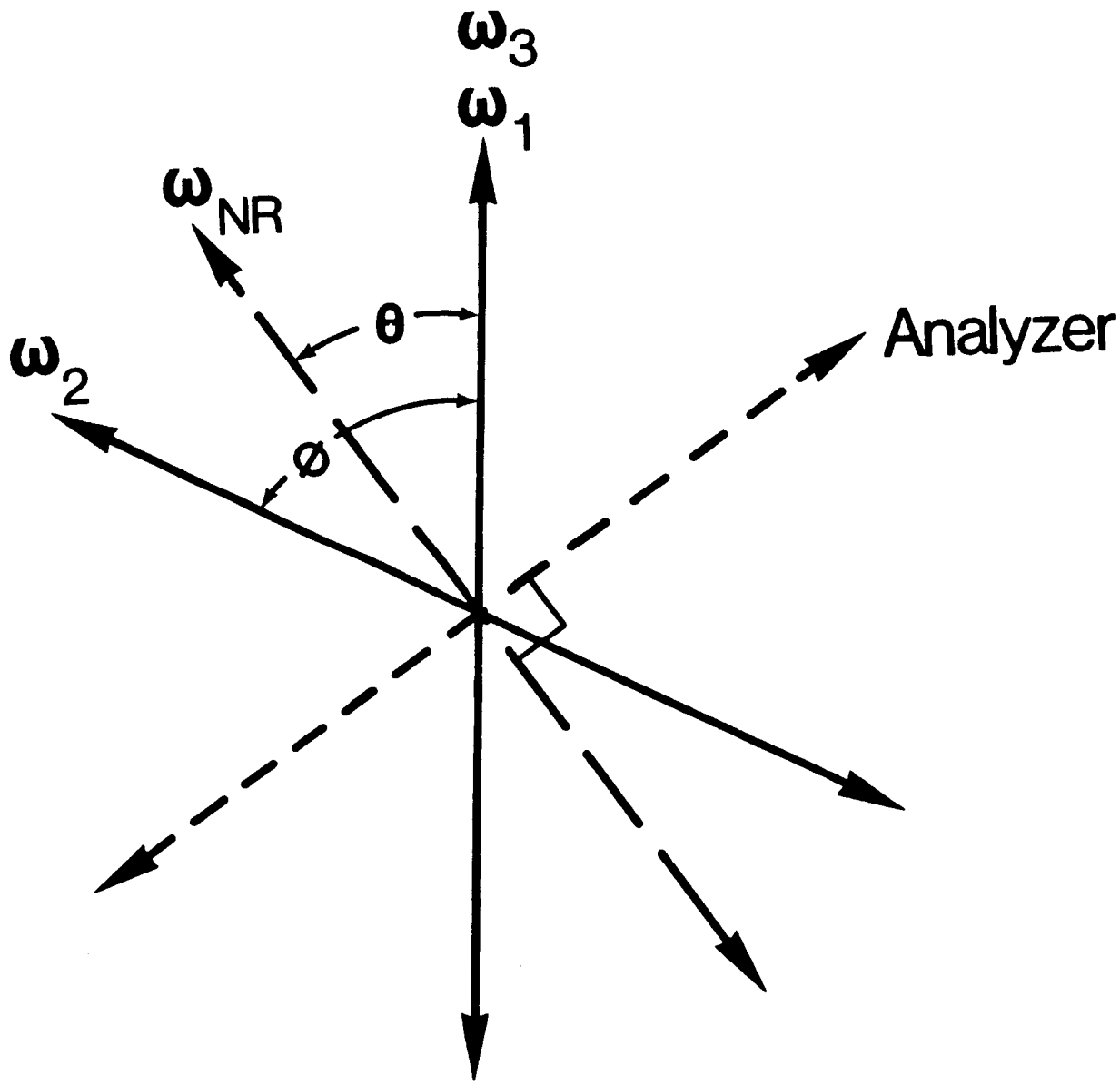

Figure 3. Polarization configuration required for rejection of nonresonant background. $\phi = 30^{o}$, $\theta = 60^{o}$.

polarization axis. Some rejection of the resonant signal occurred in this configuration since the analyzer and resonant-polarization axis were separated by 60 deg.

Bandpass filters were used to block stray light from the PMTs. Some initial complications were found due to the large bandpass of these filters.[32] A rotational hydrogen line (5 - 7) was passed by these broad rejection filters and detected by the oxygen PMTs. This signal was eliminated through the use of narrower bandpass rejection filters.

System Calibration

The accuracy and precision of the CARS measurements were demonstrated by use of a flat-flame burner. This burner had been studied previously and found to be characterized by a well-behaved temperature profile.[15] The burner, produced by McKenna Industries, Inc., was composed of a 7.94-cm-diam. sintered-stainless-steel plug housed in a stainless-steel jacket. The burner was cooled by a water coil within the plug. The burner was operated with the air flow held constant at 100 ℓ/min and the hydrogen flow adjusted over the stoichiometric fraction range of $\sim$ 0.1 - 1.0. The water flow rate and temperature rise as well as the hydrogen and air flow rates were measured and recorded by the computer system. These experimental values were used to calculate the expected temperature and species concentrations in the flow.[33]

Figure 4 shows the comparison of the CARS and calculated values for temperature, nitrogen number density, and oxygen number density. The CARS values shown represent the mean of 100 data shots. The oxygen measurements have a minimum detectable limit of $\sim 1 \times 10^{17}$ molec./cc due to the interaction of the nonresonant and resonant susceptibility which could not be completely eliminated because of incomplete polarization of the laser beams.

The relationship between the intensity in the data legs and reference legs was also required for accurate calculation of species concentration. This was accomplished by acquiring data with ambient air in both the data and the reference sample volumes.

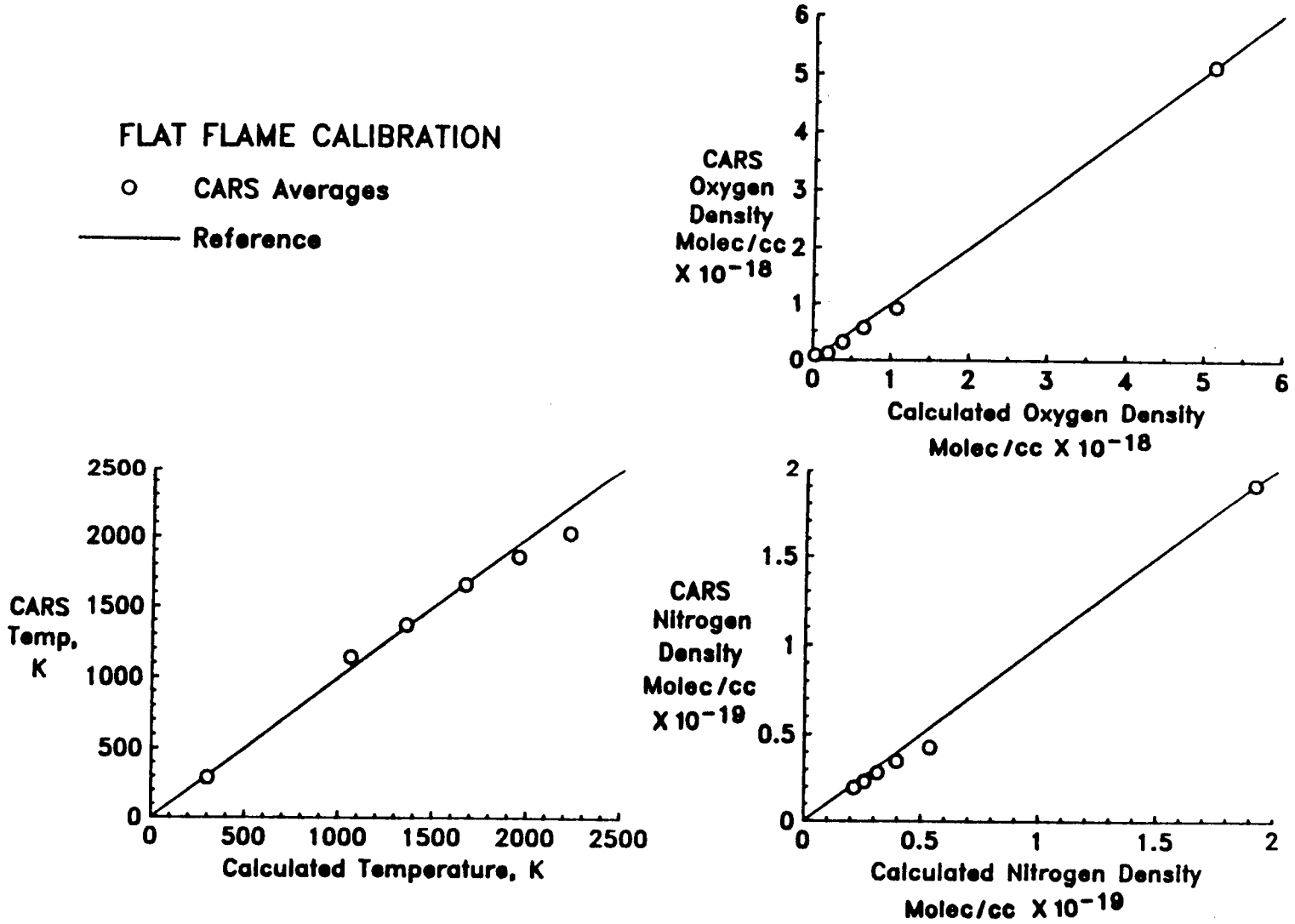

Figure 4. Calibration data from flat-flame burner.

COMPUTER CONTROL

A complete description of the computer control of the Reticon detector has been given previously;[16] therefore, only a summary will be given here. The multichannel detector used in this system was an EG&G PAR 1420 Reticon. This detector contains 1024 individual diode elements, the center 700 of which were preceded by a fiber-optic-coupled, proximity-focused, microchannel plate intensifier. An EG&G PAR 1218 Detector Controller was used for electronic control of the scanning and data acquisition of the detector. A Reticon interface was specially built to communicate with the diode-array controller. This interface handles separate input and output data lines, signal drivers for long-distance operation, and the inverted logic required by the controller.

Scanning of the Reticon was controlled by random-access memory (RAM) within the 1218 controller. This memory provided each individual detector element (pixel) with predefined scanning instructions. These instructions were calculated by the MODCOMP and downloaded into the 1218. This instruction set fast scans over the unintensified portion of the detector and provided normal analog-to-digital conversion over the center 700 pixels.

An assembly-language program was written to initiate the Reticon scanning. At the beginning of each scan cycle, a signal was sent from the 1218 to fire the laser. Three complete scans of the Reticon were accomplished between laser shots. The first was the data-acquisition scan, and other two were used to clean the pixels of any remaining signal before the next laser firing. During these "clean scans" the data were transferred to magnetic tape for processing.

Collection of photomultiplier data was also triggered by the laser pulse and, therefore, occurred simultaneously with the Reticon scans. A Kinetics 1500 CAMAC Crate was used to house the PMT collection electronics. The PMT signals were sent to a LeCroy 2249SG 12-Channel Analog-to-Ditigal Converter. This unit was triggered with a LeCroy 2323 Programmable Dual Gate Generator. These signals were routed to the MODCOMP via an IEEE interface and stored on magnetic tape with the Reticon data.

An additional program was run simultaneously with the data-acquisition program to produce a real-time display of several system parameters. In particular, burner flow conditions and PMT output were displayed. The Reticon output was displayed on an oscilloscope.

Data Reduction

To obtain the temperature, the experimental nitrogen spectra were compared with a library of precalculated theoretical spectra. These spectra were calculated in 20-K steps and stored on disk. The experimental data were retrieved from tape and corrected with a background data scan and a detector response function. The computer then selected the largest unsaturated sample from the three nitrogen data signals. The data were compared with a library of precalculated theoretical spectra to obtain the experimental temperature.

Once the temperature had been obtained, the concentrations of nitrogen and oxygen were extracted. The number density N of a species at temperature t has been shown[30] to be

$$N_t = N_{300}\{(I_t/I_{300})(I_{t,calc}/I_{300,calc})\}^{1/2} \qquad (4)$$

where N_{300} is the number density at 300 K; I_t is the experimental integrated intensity corrected for reference fluctuations; and I_{300} is the integrated intensity at 300 K, obtained from a calibration run in room air. The calculated values were generated from the precalculated spectral library.

The experimental nitrogen integrated intensity was obtained by summing the spectral channels selected by the fitting routine. Oxygen density calculations were simplified by the use of photomultiplier tubes which yield integrated intensity directly. A time of $\sim$ 2.5 s was required for analysis of each measurement on the MODCOMP computer. The arithmetic mean, standard deviation, and 95% confidence level were calculated for each data set (100 laser shots) for comparison with CFD calculations.

CARS Signal Errors

Errors must be considered which were associated with signal generation and signal detection. The most prevalent error associated with the CARS system is the fluctuation in the laser outputs. First, the YAG laser intensity varies considerably from shot to shot. Since this laser is used to pump the dye lasers, this variability is transferred to their output. Also, temperature changes in the doubling crystals effected a long-term change in the intensity output. A temperature-stabilization unit was installed on the primary doubling crystal to reduce this effect. In addition, referencing of the generation efficiency was used in this system to compensate for this type of fluctuation. The spectral character of the broadband dye lasers was dependent upon the fluorescence and absorption of the dye used. However, because of the competition among the many available modes, the output was very structured and variable. This type of fluctuation cannot be tracked adequately by referencing and constituted a major source of noise.

In the current system, four laser beams were focused and crossed to form the sample volume. When sampling is conducted in the center of a turbulent environment, considerable beam steering may occur prior to the focus. This steering causes random misalignment of the beams and subsequent random decrease in signal intensity. As the signal beams exit through the sample, beam steering may occur again. This steering may move the beam on the detection optics and alter the collection efficiency.

The size and position of the sample volume was also critical to the interpretation of the data. In the burner studied, eddies of reactants and products form and move downstream. These eddies have a broad size range. If the sample volume is larger than the eddy size, an averaging of the temperature and densities will occur, and true point measurements will not be possible. In addition, if the sample volume is positioned such that it measures two different flows (i.e., fuel and coaxial air), a weighted averaging will occur. It should be noted that a tradeoff exists between sample-volume size and absolute signal intensity.

The nonresonant signal can be a source of error. The nitrogen analysis software assumed that the nonresonant signal was relatively low and, therefore, handled in the data reduction. The oxygen system, because of the relatively low oxygen density, utilized polarization rejection of the nonresonant background. This technique requires excellent polarization characteristics in the lasers and optics for achievement of complete rejection. In this system distortions in the polarization characteristics of the laser beams were introduced by the large number of optical elements through which the laser beams had to pass. Therefore, the possible incomplete rejection of nonresonant background limited the minimum oxygen level detected.

The narrow filter used before the oxygen PMTs to reject an interfering hydrogen line (see above) may have distorted the lineshape of the oxygen signal. This distortion could have caused an error in the oxygen-density calculation since it is dependent upon a known lineshape. The errors associated with the Reticon detector used in the nitrogen leg have been well documented.[18] These errors were found to be due mainly to saturation of the image intensified on the front end of the photodiode array.

CARS DATA-REDUCTION ERRORS

The theoretical description of the CARS process was continuously being refined to fit the experimental data more accurately. These improvements are generally not needed for such low-resolution studies. However, they may introduce finite errors and, therefore, are discussed here. In this system the nonresonant-background term was assumed to be a simple function of constituent densities which were adiabatically calculated from the experimental temperature. The nonresonant values of Rado[34] were used. These values have been disputed by Hall.[35] Recently, more complex fits which include the nonresonant background as a variable have also been attempted with success.[36] This system also assumed that the Raman linewidth follows a simple 1/T function. Rahn has shown that this assumption is an oversimplification.[37] The theoretical spectra must be convolved with the system laser and detector linewidth functions. The convolutions of Yuratich[38] have been used for this system.

Recently, Teets[39] and Katolica[40] introduced an improved convolution which more accurately takes into account the nonresonant interference. The library interval (20 deg.) also imposes a lower limit on the reduced data.

SUBSONIC DIFFUSION BURNER

The burner used in the present studies consisted of two coaxial tubes. The inner tube, which carried the fuel, had a 4.7-mm inner diameter and a 6.4-mm outer diameter. This tube was tapered at the exit plane to a lip thickness of 0.51 mm. The outer tube, which carrried air, had an inner diameter of 24.5 mm. The length of the burner was $\sim$ 45 cm. Typical flow rates were 100 m/s in the air tube and 15 m/s in the fuel tube. The fuel consisted of a mixture of 80% hydrogen and 20% nitrogen. The addition of nitrogen to the fuel was necessitated by the use of nitrogen as the temperature probe species.

Figure 5 displays a spark shadowgraph of this burner under the above-stated flow conditions. This obviously very turbulent flow provided a good test of the dynamic range of the CARS system. Fast photography of this flow reveals the formation of large eddys which break up further downstream.

The subsonic burner was mounted on a motorized X-Z translational system. The Y-axis (along the laser beams) was adjustable but not motorized. This system effectively allows the sample volume to move through various positions of the flame without alignment difficulties.

The normal acquisition sequence began with a calibration run in ambient air. After the burner had been started and stabilized, a background run was made. Each data point was the accumulation of 100 laser shots. During the background run the dye-laser beams were blocked to allow only stray light to enter the detectors. The burner was then positioned by means of the motorized translational stages, and a CARS data point was obtained. One additional background point was obtained for approximately every five data points.

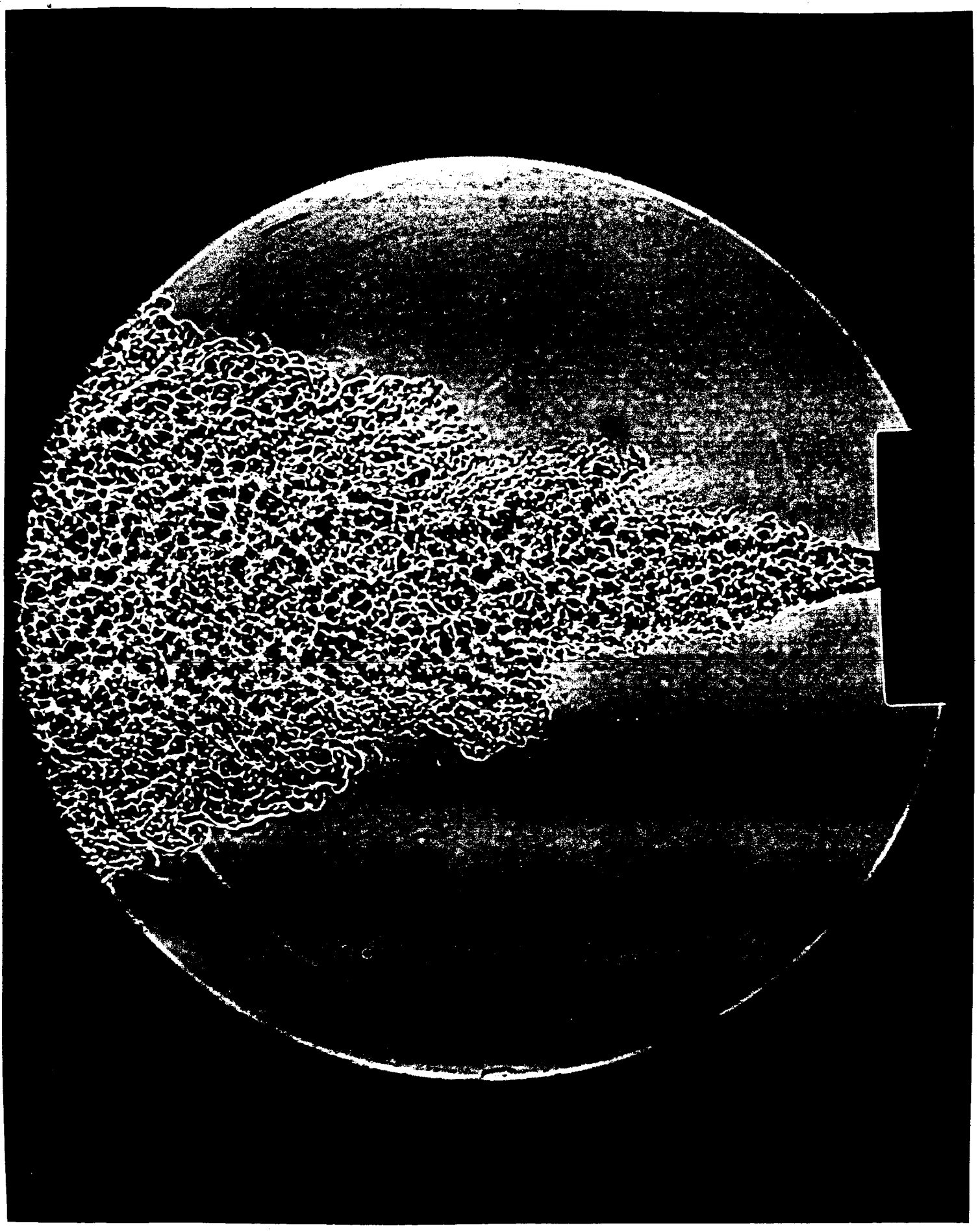

Figure 5. Shadowgraph of combustion produced by coaxial diffusion burner.

An axial profile and two radial profiles were obtained above the coaxial burner. The axial profile began as close to the jet exit as physically possible and extended 35 fuel-jet diameters downstream (Fig. 6). The radial surveys were located at 5.5 and 22.1 fuel-jet diameters downstream (Figs. 7 and 8). These radial profiles began at the center line and extended 5 fuel-jet diameters to the outer portion of the flame.

COMPUTATIONAL FLUID DYNAMICS

The major application of the CARS results to date has been in the validation of computational-fluid-dynamics (CFD) computer-modeling codes. Considerable effort has been placed on generating codes for predicting complex combustion environments. CARS measurements provide experimental data which can be used to refine the numerous adjustable parameters found in these codes. Initially, two separate codes were used with the data. The first, a modification of a CHARNAL code,[41] solves parabolized Navier-Stokes equations using a marching finite-difference algorithm and includes a two-equation turbulence model ($k - \varepsilon$). Combustion was modeled by hydrogen-oxygen equilibrium chemistry, with the nitrogen being treated as inert. Input to the code consisted of velocity, fuel mass fraction, turbulent kinetic energy, static temperature, and static pressure at the initial station located 0.01 fuel-jet diameters downstream of the exit plane. Initial velocity and turbulence intensity profiles were obtained with a hot-wire anemometer using cold-air flows. Initial profiles of static temperature and pressure were assumed to be uniform over both jets at 300 K and 1 atm. Equilibrium chemistry assumes that the local mixture reacts instantaneously to an equilibrium mixture of products; this assumption is typically used with low flow rates.

The second computational method used was the TEACH code, which is a modified version of the REACT2D[42] code. The code solves the elliptical time-averaged Navier-Stokes equations using the k-ε turbulence model for two-dimensional reacting flows. The eddy-breakup combustion model of Magnussen and Hjertager[43] was used; this model relates the combustion of fuel to the breakup and mixing of turbulent eddies and the mean concentration of reacting species. A solid wall located at 4 jet diameters was used to approximate the air boundary. The law of the wall velocity

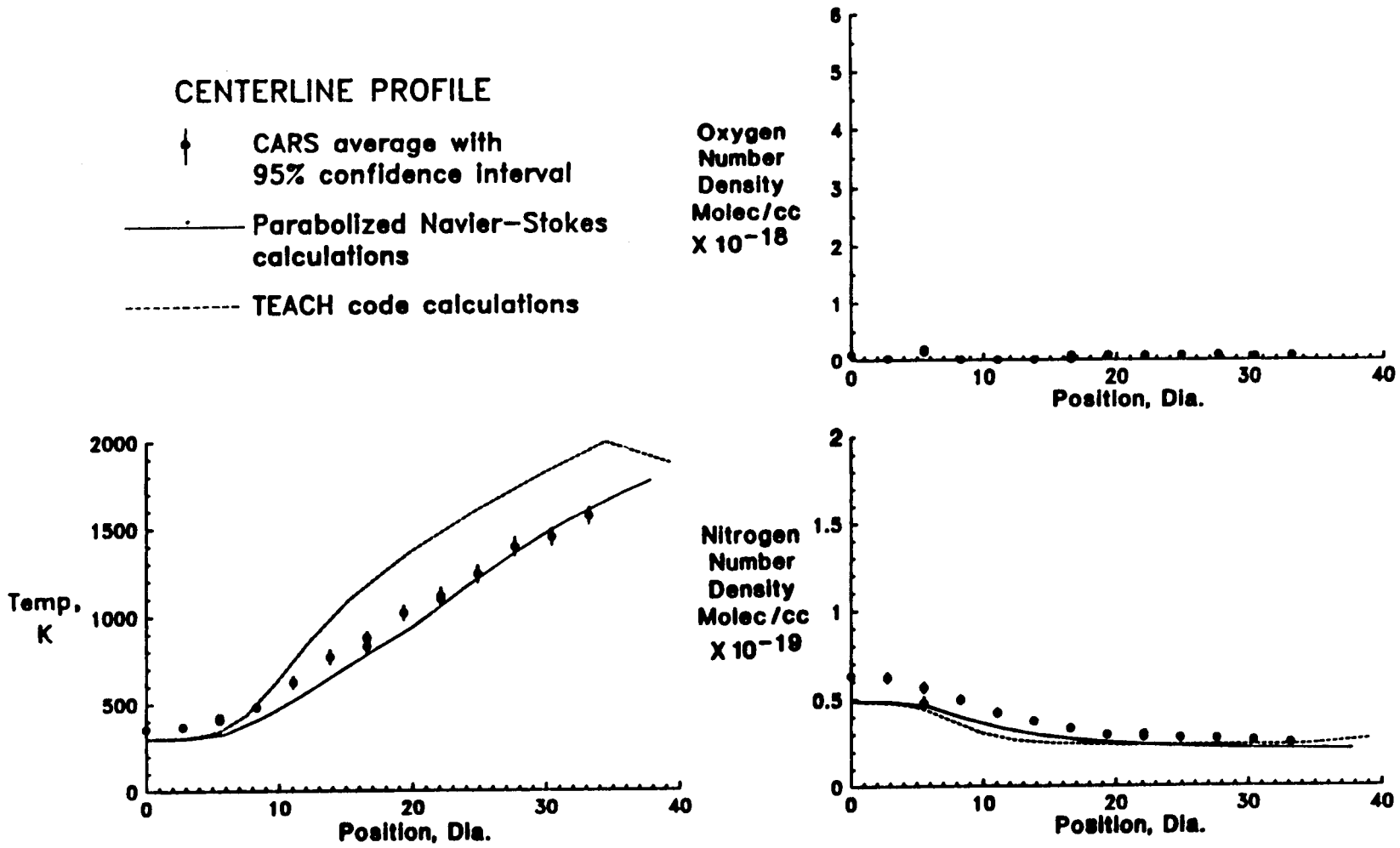

Figure 6. CARS data and CFD calculation along centerline.

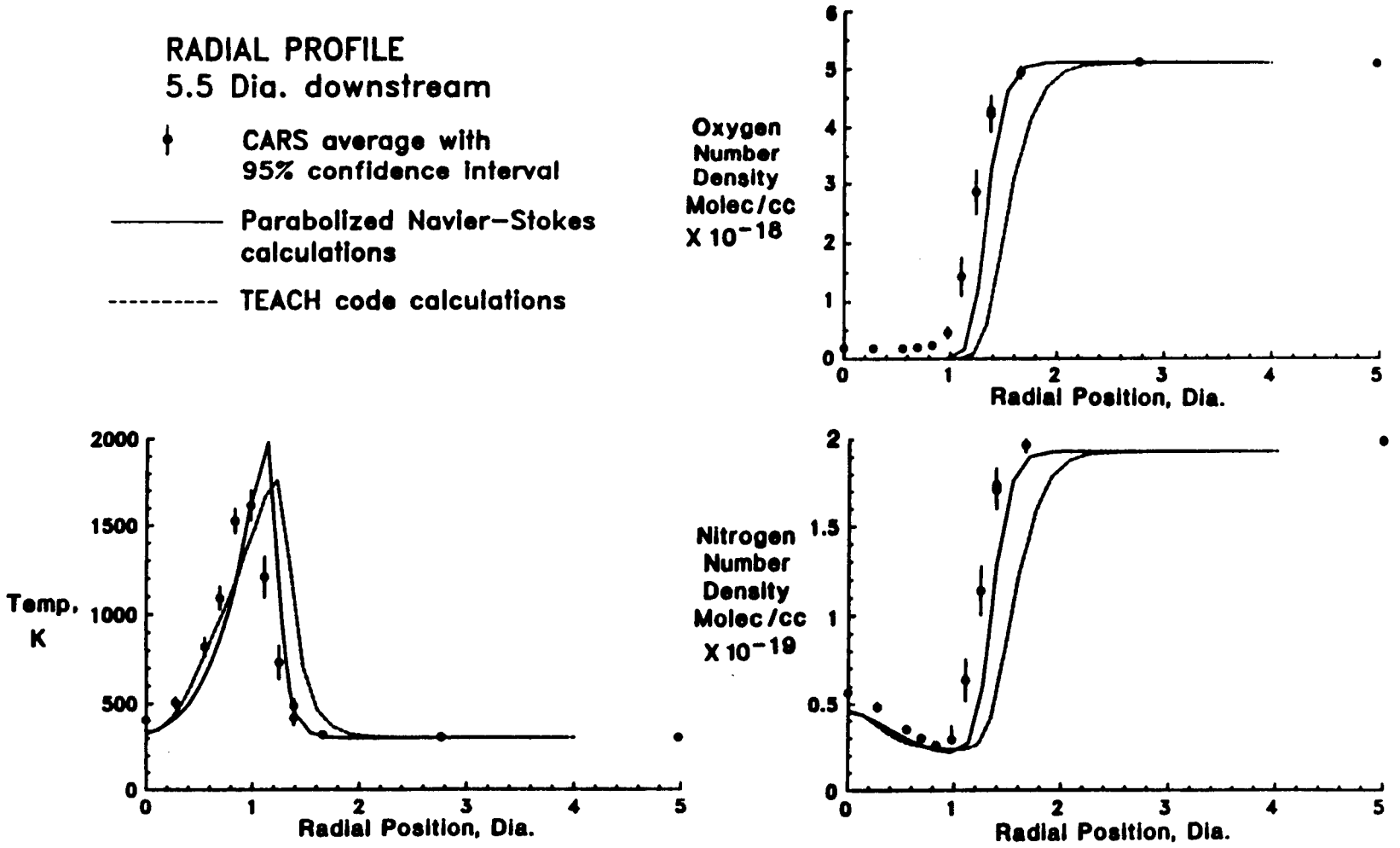

Figure 7. CARS data and CFD calculations from radial profile 5.5 jet diameters downstream.

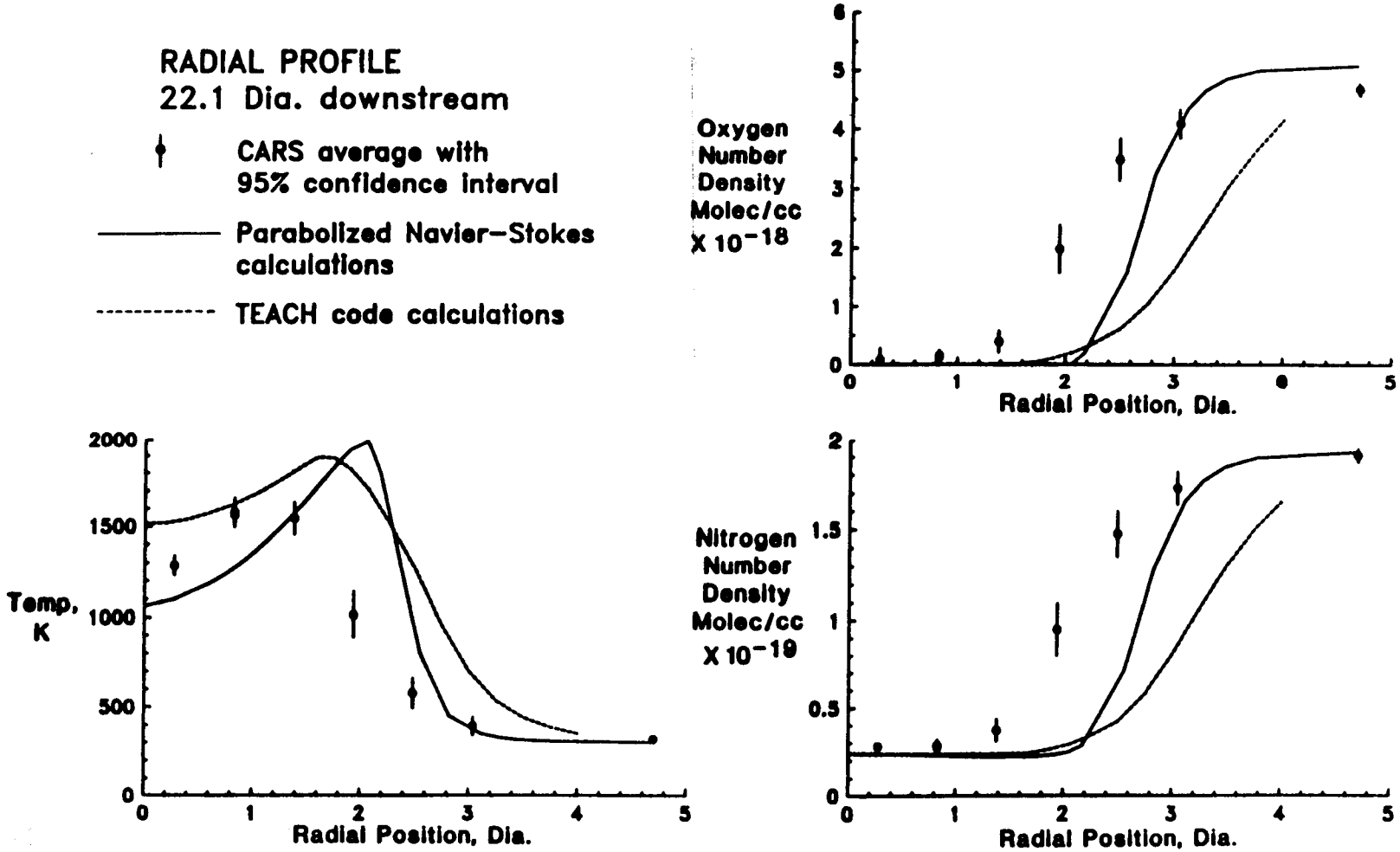

Figure 8. CARS measurements and CFD calculations from radial profile 22.1 jet diameters downstream.

profile was used. At the outlet, axial gradients of all variables except velocity were assumed to vanish. The TEACH code iterated until the nondimensional residual was minimized.

In general, the correlation between the CARS data and the data generated by the CFD codes was very good. The major differences were in the flame-spreading rate and the peak temperature. These deviations are readily explainable by the assumptions built into the CFD codes. Two factors may contribute to this deviation--an overprediction of the heat release and an overprediction of the mixing rate. The heat release may be over-predicted for two reasons. First, the equilibrium model may not adequately model the real system which has finite reaction rates. Secondly, these codes do not include a complete coupling model between turbulence and the chemical reaction. The mixing rate may have been overpredicted for three additional reasons. First, numerical diffusion can cause numerical smearing; this effect was suspected to be minor since the flow was aligned along the mesh and refinements to the grid had only small effects upon the results. Secondly, the turbulence model itself, even for nonreacting flows, overpredicted the mixing of the jet. Thirdly, as the jet reacts, a low-density "buffer region" forms in the shear layer; the turbulence model did not account for the dynamic effects of this variable density.

The CHARNAL code appears to furnish more accurate predictions of the mixing as indicated by the relatively close correlation between the experimental and calculated data in the axial profile and the lower predicted spreading rate in the radial profiles. However, the peak temperatures calculated by the TEACH code more closely match the experimental data. The lower peak temperature may be the result of the use of the eddy-breakup model. This model will weakly link the chemistry and turbulence, thereby preventing the system from obtaining the "equilibrium" temperature value.

SUMMARY

A nonintrusive diagnostic system has been developed around a coherent anti-Stokes Raman spectroscopy instrument. This system is capable of

measuring temperature and nitrogen and oxygen number densities in turbulent combustion environments. High temporal and spatial resolution, luminosity discrimination, and a large dynamic range are important advantages of this system. Turbulent subsonic flow has been investigated with this system.

REFERENCES

1. N. Hata; A. Matsuda; K. Tanaka; K. Kajiyama; N. Maro; and K. Sajiki: "Detection of Neutral Species in Silane Plasma Using Coherent Anti-Stokes Raman Spectroscopy," Japanese Journal of Applied Physics, Vol. 22, 1983, p. L1.

2. W. F. Lynn; P. P. Yaney; L. P. Goss; and S. W. Kizirnis: "Plasma Diagnostics Using Coherent Anti-Stokes Raman Spectroscopy," A.I.P. Conference Proceedings, Vol. 146, 1986, p. 277.

3. G. C. Alessandretti; and P. Violino: "Thermometry by CARS in an Automobile Engine," Journal of Physics D: Applied Physics, Vol. 16, 1983, p. 1583.

4. D. Klick; K. A. Marko; and L. Rimai: "Broadband Single-Pulse CARS Spectra in a Fired Internal Combustion Engine," Applied Optics, Vol. 20, 1981, p. 1178.

5. Y. Matsumoto; H. Matsui; and T. Asaba: "Measurement of CARS Intensity in Hydrogen Molecule Behind Shock Wave," Transactions of the Japan Society for Aeronautical and Space Sciences, Vol. 26, No. 73, Nov. 1983, p. 131.

6. K. Knapp; and F. J. Hindelang: "Measurement of Temperature in a Shock Tube by Coherent Anti-Stokes Raman Spectroscoy (CARS)," Proceedings of the 13th International Symposium on Shock Tubes and Waves, State University of New York Press, Albany, New York, July 1981, p. 132.

7. L. P. Goss; B. G. McDonald; D. D. Trump; and G. L. Switzer: "CARS Thermometry and N_2 Number Density Measurements in a Turbulent Diffusion Flame," in "Combustion Diagnostics by Nonintrusive Methods," eds. J. A. Roux and T. D. McCay, Vol. 92 of Progress in Astronautics and Aeronautics 1984, p. 24.

8. A. C. Eckbreth; G. M. Dobbs; J. H. Stufflebeam; and P. A. Tellex: "CARS Temperature and Species Measurements in Augmented Jet Engine Exhausts," Applied Optics, Vol. 23, No. 9, May 1, 1984, p. 1328.

9. A. Farrio; M. Garbi; and C. Malvicini: "Real Time CARS Spectroscopy in a Semi-Industrial Furnace," Centro Inforcizioni Studi Esperienze (CISE), Milan, Italy, Report 2042, 1983.

10. G. L. Switzer; L. P. Goss; D. D. Trump; C. M. Reeves; J. S. Stutrud; R. P. Bradley; and W. M. Roquemore: "CARS Measurements in the Near-Wake Region of an Axisymmetric Bluff-Body Combustor," presented at the AIAA/SAE/ASME/-ASEE 21st Joint Propulsion Conference, Monterey, CA, July 8-10, 1985, AIAA-85-1106.

11. E. J. Beiting: "Multiplex CARS Temperature Measurements in a Coal-Fired MHD Environment," Applied Optics, Vol. 25, No. 10, May 15, 1986, p. 1684.

12. B. Attal; M. Pealat; and J. P. Taran: "CARS Diagnostics of Combustion," presented at the AIAA 18th Aerospace Sciences Meeting, Pasadena, CA, Jan. 14-16, 1980, AIAA-80-0282.

13. M. Alden; and S. Wallin: "CARS experiments in a Full Scale (10 X 10 m) Industrial Coal Furnace," Applied Optics, Vol. 24, No. 21, November 1, 1985, p. 3434.

14. T. J. Anderson; I. W. Kay; and W. T. Peschke: "CARS Feasibility Demonstration in Supersonic Combusting Flows," presented at the 22nd JANNAF Combustion Meeting, Pasadena, CA, October 7-10, 1985, CPIA Publication 439, p. 417.

15. R. R. Antcliff; and O. Jarrett, Jr.: "Comparison of CARS Combustion Temperatures with Standard Techniques" in "Combustion Diagnostics by Nonintrusive Methods," eds. J. A. Roux and T. D. McCay, Vol. 92 of Progress in Astronautics and Aeronautics 1984, p. 45.

16. J. R. Posenau; and R. R. Antcliff: "Multichannel Detector Control with a MODCOMP Computer," presented at the Americas Annual MUSE Meeting, Ft. Lauderdale, FL., Dec. 4-9, 1983.

17. R. R. Antcliff; O. Jarrett, Jr.; and R. C. Rogers: "CARS System for Turbulent Flame Measurements," Journal of Propulsion and Power, Vol. 1, No. 3, May-June 1985, p. 205.

18. R. R. Antcliff; M. E. Hillard; and O. Jarrett, Jr.: "Intensified Silicon Photodiode Array Detector Linearity: Application to Coherent Anti-Stokes Raman Spectroscopy," Applied Optics, Vol. 23, No. 14, July 15, 1984, p. 2369.

19. W. M. Tolles; J. W. Nibler; J. R. McDonald; and A. B. Harvey: "A Review of the Theory and Application of Coherent Anti-Stokes Raman Spectroscopy (CARS)," Applied Spectroscopy, Vol. 31, No. 4, 1977, p. 253.

20. R. N. DeWitt; A. B. Harvey; and W. M. Tolles, "Theoretical Development of the Third-Order Susceptibility as Related to Coherent Anti-Stokes Raman Spectroscopy (CARS)," NRL Memorandum Report 3260, April 1976.

21. H. Lotem; R. T. Lynch; and N. Bloembergen, "Interference Between Raman Resonances in Four-Wave Difference Mixing," Physical Review A, Vol. 14, No. 5, November 1976, p. 1748.

22. L. P. Goss; and P. W. Schreiber: "Assessment of the Application of CARS to Combustion Diagnostics," Proceedings of the International Conference on LASERS '80, 1980, p. 220.

23. J. F. Verdieck; R. J. Hall; and A. C. Eckbreth: "Electronically Resonant CARS Detection of OH," in "Combustion Diagnostics by Noninstrusive Methods," eds, J. A. Roux and T. D. McCay, Vol. 92 of Progress in Astronautics and Aeronautics 1984, p. 58.

24. L. A. Carreira; and R. R. Antcliff: "Applications of Resonance Enhanced CARS," in "Advances in Laser Spectroscopy," Vol. 1, Chap. 6, 1982, p. 121.

25. F. Moya; S. Druet; and M. Pealat: "Flame Investigation by Coherent Anti-Stokes Raman Scattering," presented at the AIAA 14th Aerospace Sciences Meeting, Washington, D.C., January 26-28, 1976, AIAA-76-29.

26. W. B. Roh; P. W. Schreiber; and J. P. E. Taran: "Single-Pulse Coherent Anti-Stokes Raman Scattering," Applied Physics Letters, Vol. 29, No. 3, August 1, 1976, p. 174.

27. Y. Prior: "Three-Dimensional Phase Matching in Four-Wave Mixing," Applied Optics, Vol. 19, No. 11, June 1, 1980, p. 1741.

28. J. A. Shirley; R. J. Hall; and A. C. Eckbreth: "Folded BOXCARS for Rotational Raman Studies," Optics Letters, Vol. 5, No. 9, September 1980, p. 380.

29. L. P. Goss; G. L. Switzer; and P. S. Schreiber: "Flame Studies with the Coherent Anti-Stokes Raman Spectroscopy Technique," Journal of Energy, Vol. 7, No. 5, May 1983, p. 389.

30. L. P. Goss; D. D. Trump; B. G. McDonald; and G. L. Switzer: "10-Hz Coherent Anti-Stokes Raman Spectroscopy Apparatus for Turbulent Combustion Studies," Review of Scientific Instruments, Vol. 54, No. 5, May 1983, p. 563.

31. L. A. Rahn; L. J. Zych; and P. L. Mattern: "Background-Free CARS Studies of Carbon Monoxide in a Flame," Optics Communications, Vol. 30, No. 2, August 1979, p. 249.

32. R. R. Antcliff; O. Jarrett, Jr.; R. C. Rogers; and T. VanOverbeck: "Multispecies in Turbulent Combustion," presented at the 23rd JANNAF Combustion Meeting, Hampton, VA, October 20-24, 1986.

33. V. R. Mascitti: "A Simplified Equilibrium Hydrogen-Air Combustion Gas Model for Use in Air Breathing Engine Cycle Computer Progress," NASA TN D-4747, 1968.

34. W. G. Rado: "The Nonlinear Third Order Dielectric Susceptibility Coefficients of Gases and Optical Third Harmonic Generation," Applied Physics Letters, Vol. 11, No. 4, August 1967, p. 123.

35. R. J. Hall: "Theoretical Modeling of the CARS Spectra of Combustion Molecules," Proceedings of the International Conference on Lasers, published by S.R.S. Press, McLean, VA, 1982, p. 726.

36. R. J. Hall; and C. R. Boedecker: "CARS Thermometry in Fuel-Rich Combustion Zones," Applied Optics, Vol. 23, No. 9, May 1, 1984, p. 1340.

37. L. A. Rahn; A. Owyoung; M. E. Coltrin; and M. L. Koszykowski: "The J Dependence of Nitrogen 'Q' Branch Linewidths," Proceedings of the VIIth International Raman Conference, published by North Holland, NY, 1980, p. 694.

38. M. A. Yuratich: "Effects of Laser LInewidth on Coherent Anti-Stokes Raman Spectroscopy," Molecular Physics, Vol. 38, No. 2, 1979, p. 625.

39. R. Teets: "Accurate Convolutions of CARS Spectra," Optics Letters, Vol. 9, No. 6, June 1984, p. 226.

40. H. Kataoka; S. Maeda; and C. Hirose: "Effects of Laser Linewidth on the Coherent Anti-Stokes Raman Spectroscopy Spectral Profile," Applied Spectroscopy, Vol. 36, 1982, p. 565.

41. D. B. Spalding; B. E. Launder; A. P. Morse; and G. Maples: "Combustion of Hydrogen-Air Jets in Local Chemical Equilibrium (A Guide to the CHARNAL Computer Program)," NASA CR-2407, June 1974.

42. L. M. Ciapetta: "Users Manual for a TEACH Computer Program for the Analysis of Turbulent, Swirling Flow in a Research Combustor," United Technologies Research Center Report R83-915540-27, 1983.

43. B. F. Magnusen; and B. H. Hjertager: "On Mathematical Modeling of Turbulent Combustion with Special Emphasis on Soot Formation and Combustion," presented at the Sixteenth Symposium (International) on Combustion, The Combustion Institute, 1978, p. 719.

Standard Bibliographic Page

1. Report No.	2. Government Accession No.	3. Recipient's Catalog No.
NASA CR-178245		

4. Title and Subtitle	5. Report Date
APPLICATION OF CARS TO SCRAMJET COMBUSTION	April 1987
	6. Performing Organization Code

7. Author(s)	8. Performing Organization Report No.
R. R. Antcliff	6657 Final
	10. Work Unit No.

9. Performing Organization Name and Address	11. Contract or Grant No.
Systems Research Laboratories, Inc. Research Applications Division 2800 Indian Ripple Road Dayton, OH 45440-3696	NAS1-16562
	13. Type of Report and Period Covered
12. Sponsoring Agency Name and Address National Aeronautics and Space Administration Washington, DC 20546	Contractor Report
	14. Sponsoring Agency Code

15. Supplementary Notes

Langley Technical Monitor: G. Burton Northam
Final Report

16. Abstract

A coherent anti-Stokes Raman spectroscopic (CARS) instrument has been developed for measuring simultaneously temperature and N_2 - O_2 species concentration in hostile flame environments. A folded BOXCARS arrangement was employed to obtain high spatial resolution. Polarization discrimination against the nonresonant background decreased the lower limits of O_2 detectivity. The instrument has been primarily employed for validation of computational fluid-dynamics computer-model codes. Comparisons have been made to both the CHARNAL and TEACH codes on a hydrogen diffusion flame with good results.

17. Key Words (Suggested by Authors(s))	18. Distribution Statement
coherent anti-Stokes Raman spectroscopy, CARS, nonintrusive diagnostics, non-linear Raman spectroscopy, combustion diagnostics	Unclassified - Unlimited

19. Security Classif.(of this report)	20. Security Classif.(of this page)	21. No. of Pages	22. Price
Unclassified	Unclassified	34	

For sale by the National Technical Information Service, Springfield, Virginia 22161